

Templated assembly of metal nanoparticle films on polymer substrates

R. F. Waters¹, A. Ohtsu^{1,2}, M. Naya², P. A. Hobson³, K. F. Macdonald¹ and N. I. Zheludev^{1,4}¹ Optoelectronics Research Centre & Centre for Photonic Metamaterials, University of Southampton, Southampton, SO17 1BJ, UK² Frontier Core Technology Laboratories, Fujifilm Corporation, 577 Ushijima Kaisei-machi, Ashigarakami-gun Kanagawa, 258-8577, Japan³ QinetiQ Ltd., Cody Technology Park, Farnborough, Hampshire GU14 0LX, UK⁴ Centre for Disruptive Photonic Technologies, School of Physical and Applied Sciences & The Photonics Institute, Nanyang Technological University, Singapore 637371

We report on directed self-assembly of ordered, vapor-deposited gallium nanoparticles on surface-relief-structured polymer substrates. Grating templates impose periodic order in one dimension, most effectively when the grating half-period is of order the mean unperturbed center-to-center particle spacing for a given mass-thickness of Ga. Self-organized order also emerges in the perpendicular direction as a consequence of the liquid-phase particles' nucleation, growth and coalescence on the ridges of the grating pattern in relative isolation from the adjacent slots, and vice versa.

With the emergence of advanced, nano-engineered (meta)materials as a key enabling technology in fields ranging from environmental remediation to electronics and photonics,¹⁻³ interest has grown in the development of scalable, high-throughput, top-down and bottom-up manufacturing processes for such materials. In this regard, self-assembly techniques hold great appeal as means to create both end-product materials themselves or intermediate structures such as etch masks. Numerous approaches to directing the assembly of many kinds of materials into many geometric/composite forms have been demonstrated. For example, micro/nano-spheres on a planar surface will spontaneously adopt a hexagonal close-packed arrangement but other arrangements can be imposed by pre-patterning the substrate;⁴ colloidal nanoparticles can be shaped and chemically functionalized to achieve specific arrangements and inter-particle spacings;⁵⁻⁷ and DNA molecules can be 'programmed' to form complex 2D and 3D lattices.⁸

With many existing and potential applications in such diverse domains as catalysis, cancer treatment, and photovoltaics,⁹⁻¹¹ the preparation of metallic nanoparticle ensembles is of particular interest and technological importance. Self-assembly has been one of the main approaches to the fabrication of spontaneously ordered and disordered nanoparticles¹²⁻¹⁸ but tends to produce randomly distributed particles with a broad range of sizes. In consequence, various post-processing procedures for manipulating particle shape, size, and size distribution (e.g. based upon high-power laser-induced evaporation, desorption, and fragmentation¹⁹⁻²¹) have been reported. It has also been shown, in the specific case of gallium nanoparticles, that low intensity laser light can regulate the nanoparticle assembly process itself – near-infrared illumination of a substrate during atomic beam deposition produces close-packed nanoparticle monolayers with a relatively narrow size distribution dependent on light intensity and deposition rate.^{22, 23}

Gallium holds particular interest in the field of nanophotonics, as an 'active plasmonic' and phase-change nonlinear medium.²⁴⁻²⁶ The contrast between the

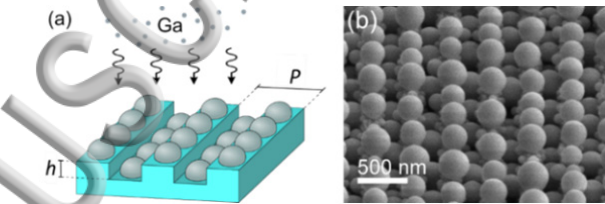


Fig. 1: Templated assembly of gallium nanoparticles. (a) Schematic illustration of the process whereby positional order is imposed by a structured substrate on particles grown via vapor deposition. (b) Scanning electron microscope image [at an oblique viewing angle] of gallium particles grown on a PET grating [$P = 600$ nm; $h = 120$ nm; Ga mass-thickness 250 nm].

optical properties of its (almost semiconductor-like²⁷) bulk solid and (nearly-free-electron metallic²⁸) liquid states, and the blue/UV plasmonic character of the latter;^{18, 29, 30} its exceptional polymorphism and its unusual phase transitional behavior under extreme conditions, e.g. in confined (interfacial or nanoparticle) geometries and/or at cryogenic temperatures³¹⁻³⁶, make it an intriguing platform from the perspective of both fundamental physics and potential applications. Here we demonstrate that the assembly of liquid-phase Ga nanoparticles during physical vapor deposition (PVD) can be directed by the nanoscale surface-relief structuring of a polymer (polyethylene terephthalate – PET) substrate (Fig. 1). We observe that control over particle size and positioning is most effectively achieved (for a given mass-thickness of deposited material) when the characteristic dimensions of the substrate structure are comparable to the center-to-center separation of particles that would be produced via self-organized growth on an unstructured substrate.

On an unstructured surface, gallium films grow in the Volmer-Weber (VW) mode, forming discrete, randomly distributed nanoparticle 'islands' rather than contiguous thin films.^{37, 38} This is indicative of the fact that the latent heat of evaporation for gallium from the PET surface is less than the latent heat of evaporation from the bulk metal – in consequence, incident atoms adhere preferentially to previously deposited gallium. The physics of VW thin film growth has been extensively

studied, though typically for solid-phase deposition, i.e. substrate temperatures below the size-effect-depressed melting points T_m^* of deposited materials, though subsequent above- T_m^* annealing has been employed as a method for the production of metallic nanoparticles.³⁹ Gallium is peculiar in this regard: Despite the fact that its 303 K bulk melting point is already unusually low for a metal, size-effects on T_m are inconsequential to the present study because the very formation of the bulk crystalline (α') phase is suppressed in the confined geometry of nano/microparticles;³³ Ga remains in the liquid state to cryogenic temperatures, solidifying in one of several ‘metastable’ crystalline forms only below ~ 255 K. The mobility of Ga atoms deposited on uncooled planar substrates thus enables growing particles to minimize surface energy by adopting a truncated spherical shape.

This behavior is analogous to the micro/macroscale condensation of water on hydrophobic surfaces and may be understood in the same terms despite the dimensional disparity of around three orders of magnitude.³⁸ Computational models of droplet accretion from vapor condensing on a surface as liquid⁴⁰ account for the evolution of their size and spatial distributions through consideration of three interacting regimes: First, the nucleation and growth of static droplets via Brownian motion of small particles on the surface; Second, coalescence of droplets as a result of individual growth bringing them into mutual contact; Third, nucleation of new droplets in voids left by coalescence. This produces a structure of larger droplets with a narrow distribution of sizes and many smaller droplets dispersed in the voids between them. As deposition progresses, mean particle radius increases linearly with time, while surface coverage increases to a saturation level of around 55%, at which point the mean inter-particle spacing for the larger sizes stabilizes. These generic models take no account of specific properties for any particular material, beyond the assumed growth kinetics, but results are consistent with the condensation of a various vapors.

In the present study, grating patterns were etched into 0.25 mm thick PET substrates by focused ion beam (FIB) milling. To prevent charging during the FIB milling process, the PET was first coated by evaporation with ~ 30 nm of gold; A symmetric, nominally rectangular grating profile was maintained over periods ranging from $P = 200$ to 1600 nm; Gratings each covered a $25 \mu\text{m} \times 25 \mu\text{m}$ area and were etched to a depth of 120 nm. (The FIB process inevitably produces lines with imperfectly vertical sidewalls and rounded corners but these deviations from the ideal rectilinear geometry of Fig. 1a are ignored as they occur on lateral scales smaller than the nanoparticle diameters.) An unpatterned reference domain of the same size was prepared by rastering the focused ion beam over the entire area to replicate any (sub)nanoscale surface roughness and gallium implantation introduced by the FIB process in the grating domains. Remaining parts of the gold anti-charging layer were then removed by wet etching (in KI/I_2 , followed by sonication in isopropyl alcohol, rinsing in deionized water and baking at 80°C for 5

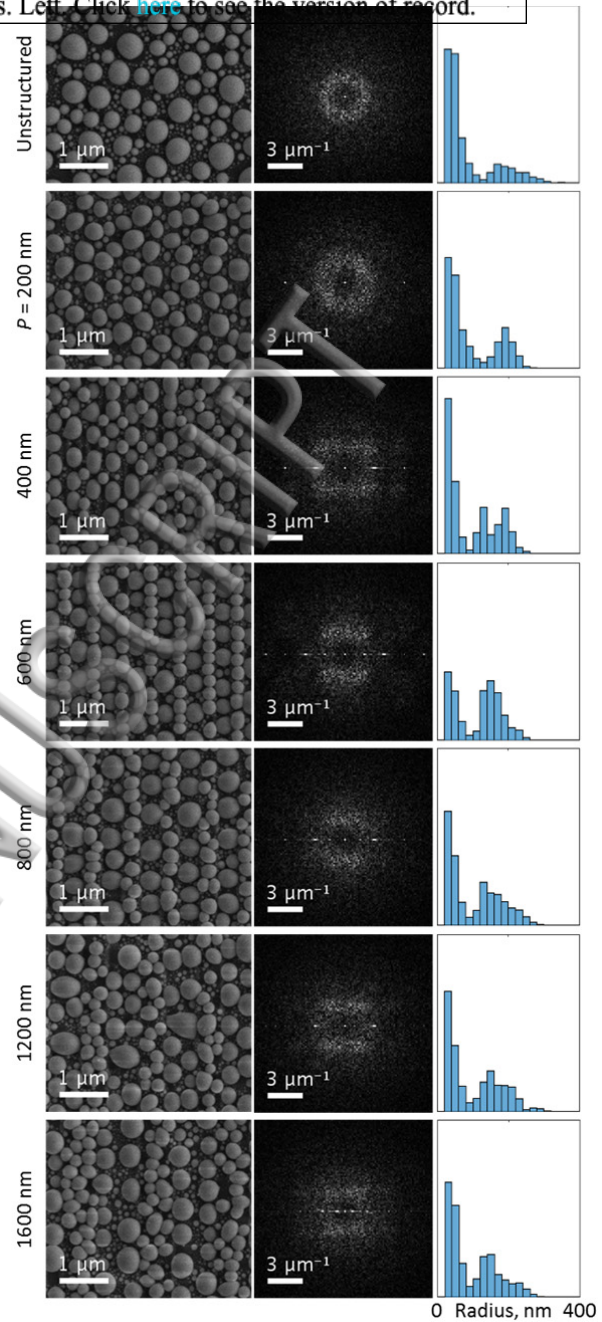


Fig. 2: Gallium nanoparticle growth on PET grating substrates. Scanning electron microscope images [left] with corresponding DFT images [center] and particle diameter histograms [right] of Ga nanoparticles [250 nm mass-thickness] grown on PET substrates patterned with symmetric, 120 nm deep rectangular gratings of varying period [as labelled], and for reference an unstructured PET substrate [top row]. [DFT images and histograms are derived from SEM images encompassing $25 \mu\text{m} \times 25 \mu\text{m}$ sample domains; DFT images are deliberately over-saturated to reveal diffuse features; particle diameters < 30 nm are not resolved in histogram evaluations, where the vertical scale is relative number density.]

minutes) and the PET was coated with a 250 nm mass-thickness of gallium (as measured on a quartz microbalance) by resistance evaporation under high vacuum ($\sim 5 \times 10^{-6}$ mBar) from a source of 6N purity.

The presence of a substrate surface relief structure has a profound effect on the distribution of gallium

Nanoparticles then formed, as illustrated (to the naked eye) by the sequence of scanning electron microscope (SEM) images in the left hand column of Fig. 2. This templated ordering of nanoparticle assembly was quantitatively characterized on the basis of these images via Fourier decomposition: First (using the Fiji image processing package⁴¹), a median filter was applied to despeckle the SEM images, and an intensity-thresholded local thickness algorithm was then employed to ‘flatten’ them, compensating for the fact that (by the nature of the secondary electron imaging process) particles located within the slots of the grating structure appear darker than those located on the ridges. This important correction ensures that subsequent analyses of the nanoparticles’ in-plane positional order are not distorted by imaging artefacts related to the out-of-plane height/depth (and aspect ratio) of substrate relief features. Binary maps of the nanoparticles are thus produced, from which discrete Fourier transform (DFT) images are obtained. These transforms, shown in the right hand column of Fig. 2, generally have two major components: a set of sharp maxima arranged in a horizontal line, reflecting nanoparticle order in the direction parallel to the grating vector (perpendicular to the lines), and a diffuse ‘halo’ representative of the particle distribution over all in-plane directions. As one would expect, only the latter halo is present when the substrate is unstructured – it has a radius corresponding to the mean center-to-center distance $\overline{d}_0 \sim 320$ nm between large particles in the film, which have a bimodal size distribution characteristic of the liquid-phase growth/coalescence process⁴⁰.

To the naked eye, the shortest period ($P = 200$ nm) grating does not obviously disrupt this random positional and bimodal size distribution. However, while the DFT halos are almost indistinguishable, the transform for the grating substrate does present a pair of bright maxima either side of the origin, indicating that some periodic order is imposed (i.e. that there is a tendency for particles to nucleate on the raised ridges of the grating), and the large diameter tail of the size distribution is truncated. The larger gratings (all having periods $P > \overline{d}_0$ the mean unstructured-substrate center-to-center particle spacing, and slot/ridge widths $\gtrsim \overline{r}_0$ the mean unstructured-substrate particle diameter) have a more pronounced effect on nanoparticle distribution. At $P = 400$ nm, periodic order in the direction of the grating vector is immediately apparent in the SEM image and manifested in the DFT by axial peaks at positions corresponding to the grating period and half-period (the former being dominant, as illustrated in Fig. 3), which presents axial cross-sections of DFT amplitude). The halo is also ‘squared off’, indicating the imposition of periodic order along the grating slots/ridges – this points to the emergence of some directional anisotropy in the interactions between neighboring particles during growth, i.e. some decoupling of the nucleation and coalescence kinetics between adjacent slots and ridges. These behaviors are even more prominent for the 600 nm grating, which has a period very close to $2\overline{d}_0$. As such, particles naturally coalesce either in a slot or on a

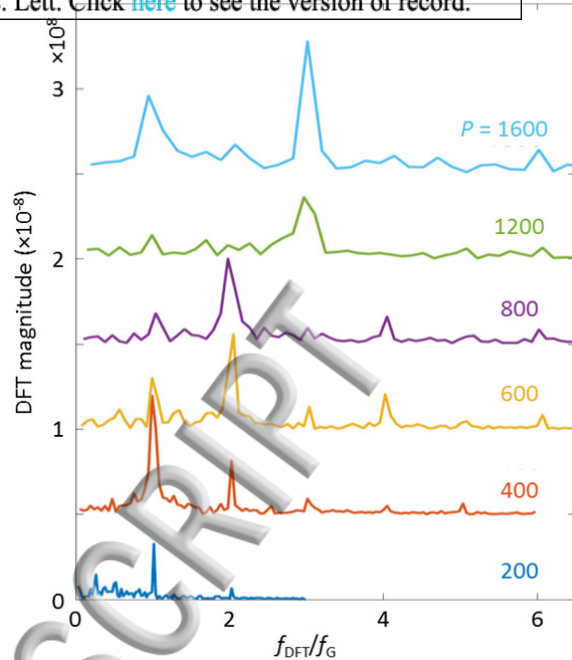


Fig. 3: Ga particle positional order in the grating vector direction. Cross-sections of DFT magnitude, as a function of frequency normalized to grating frequency f_G , along the grating vector axes of the DFT images in Fig. 2 [grating periods as labelled; Traces are vertically offset for clarity].

ridge of the structure, as reflected by the dominance of the half-period peak in the corresponding DFT cross-section of Fig. 3. The particle size distribution is also maximally perturbed at $P = 600$ nm, with a pronounced increase in the relative number density of larger particles having diameters around $P/2$. At still larger grating periods, apparent order (as to the naked eye from SEM images) diminishes and/or becomes more complex: The dominance of the half-period peak in the DFT cross-section is preserved at $P = 800$ nm but disappears at 1200 and 1600 nm as $P/2$ approaches and exceeds \overline{d}_0 .

We have focused in this study on a particular combination of grating etch depth (120 nm) and gallium mass-thickness (250 nm). At lower mass-thickness, \overline{d}_0 decreases and optimal positional templating is achieved by shorter period gratings (see Supplementary Material). For a given mass-thickness of Ga, shallower gratings exert weaker control over the positional order particles; order is maintained by deeper gratings but the secondary electron image brightness/contrast mismatch between particles in slots and on ridges becomes prohibitive to a meaningful DFT analysis.

The effect of a surface-relief nanostructured substrate on the arrangement of nanoparticles as they grown may be understood though consideration of the fact that they will seek to minimize surface free energy. For the avoidance of discontinuities in contact angle (between gallium and PET – a function of the solid/liquid/vapor interfacial free energies⁴²) and/or in the truncated spherical form of the gallium surface, particles accrete preferentially on flat areas of the substrate, rather than wrapping over the sharp edges of the slots, even when the change in substrate surface height (grating etch depth) is somewhat smaller than the particle size. (The

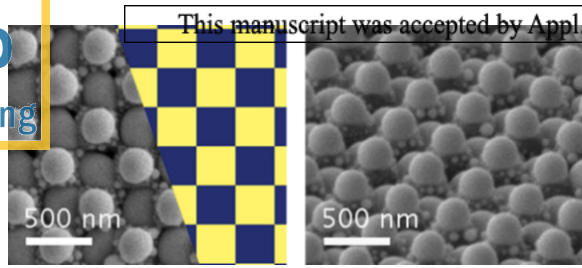


Fig. 4: 2D templating of Ga particle growth. Plan view (a) and oblique angle (b) scanning electron microscope images of Ga nanoparticles [150 nm mass-thickness] grown on a checkerboard-patterned PET substrate [a grid of 300 nm \times 300 nm squares selectively milled by FIB to a depth of 600 nm, as per the overlay in panel (a) where blue = etched and yellow = un-etched].

directionality of gallium deposition largely precludes nucleation on the near-vertical sidewalls of the grating slots.) Within the confines of this surface structural template, particle growth during PVD proceeds via the self-organized nucleation and coalescence mechanisms described above to produce ordered assemblies such as in Fig. 2. Substrate surface relief patterns may of course be designed to produce a variety of particle arrangements (of interest for example for their ensemble optical/plasmonic properties) as illustrated in Fig. 4, where self-organization is almost entirely suppressed by a checkerboard substrate that imposes 2D positional and close particle size control.

Gallium's ability to form and sustain a thin (~ 3 nm) solid oxide surface coating, even on the liquid under high vacuum,⁴³ should be noted here. Such a layer is likely to form on the nanoparticles during PVD (by reaction between the metal and substrate-adsorbed oxygen and water vapor) and may indeed account for the observed aspherical shape of some particles and the failure of some touching particles to coalesce - the latter effect in particular resulting in a surface coverage saturation level of $\sim 64\%$ somewhat higher than the 55% expected from vapor condensation models.⁴⁰

In conclusion, we have demonstrated that the growth of liquid-phase metallic (gallium) nanoparticles by vapor deposition can be controlled by surface-relief nanostructuring of the substrate. Grating and checkerboard patterns etched into polymer (PET) substrates serve as a template for the formation of one and two-dimensionally ordered assemblies of gallium particles, most effectively when the characteristic in-plane dimensions of the substrate structure (here in the few-hundred nm range) are comparable to those of the nanoparticle film that would form via unperturbed self-assembly on the unstructured substrate. In general, the nature of nanoparticle ensembles produced in this way will depend on the extent to which the deposited medium wets the substrate, the mass thickness of deposited material, and the geometry (in- and out-of-plane dimensions) of the substrate surface-relief structure. For the purposes of the present proof-of-principle study, small-area polymer templates were manufactured by focused ion beam milling, but structures at the same sub-micron scale may readily be created over much larger areas via much faster, lower-cost photo- and nanoimprint lithographic techniques, including continuously rolled

processes in the latter case.
Supplementary Material: Additional SEM and DFT images and particle size histograms, as per Fig. 2, for other gallium mass-thicknesses.

This work was supported by the Dstl through the MAST Programme, the EPSRC [grants EP/G060363/1 and EP/M009122/1], and the Singapore Ministry of Education [grant MOE2011-T3-1-005]. The data from this paper will be available from the University of Southampton repository at <http://dx.doi.org/10.5258/SOTON/399231>.

- M. M. Khin, A. S. Nair, V. J. Babu, R. Murugan and S. Ramakrishna, *Energy Environ. Sci.* **5**, 8075 (2012).
- G. Fiori, F. Bonaccorso, G. Iannaccone, T. Palacios, D. Neumaier, A. Seabaugh, S. K. Banerjee and L. Colombo, *Nat. Nanotech.* **9**, 768 (2014).
- N. I. Zheludev and Y. S. Kivshar, *Nat. Mater.* **11**, 917 (2012).
- Y. Yin, Y. Lu, B. Gates and Y. Xia, *J. Am. Chem. Soc.* **123**, 8718 (2001).
- R. W. Taylor, T.-C. Lee, O. A. Scherman, R. Esteban, J. Aizpurua, F. M. Huang, J. J. Baumberg and S. Mahajan, *ACS Nano* **5**, 3878 (2011).
- S. Sacanna, D. J. Pine and G.-R. Yi, *Soft Matter* **9**, 8096 (2013).
- A. Heuer-Jungemann, R. Kirkwood, A. H. El-Sagheer, T. Brown and A. G. Kanaras, *Nanoscale* **5**, 7209 (2013).
- A. R. Chandrasekaran and R. Zhuo, *Applied Materials Today* **2**, 7 (2016).
- G. A. Somorjai and Y. G. Borodko, *Catal. Lett.* **76**, 1 (2001).
- L. R. Hirsch, R. J. Stafford, J. A. Bankson, S. R. Sershen, B. Rivera, R. E. Price, J. D. Hazle, N. J. Halas and J. L. West, *P. Natl. Acad. Sci. USA* **100**, 13549 (2003).
- H. A. Atwater and A. Polman, *Nat. Mater.* **9**, 205 (2010).
- C. G. Granqvist and R. A. Buhman, *J. Appl. Phys.* **47**, 2200 (1976).
- V. A. Shchukin and D. Bimberg, *Rev. Mod. Phys.* **71**, 1125 (1999).
- H. Brune, *Surf. Sci. Rep.* **31**, 125 (1998).
- A. Taleb, V. Russier, A. Courty and M.-P. Pileni, *Phys. Rev. B* **59**, 13350 (1999).
- H. Brune, M. Giovannini, K. Bromann and K. Kern, *Nature* **394**, 451 (1998).
- Z. Suo and W. Lu, *J. Nanopart. Res.* **2**, 333 (2000).
- M. Yarema, M. Wörle, M. D. Rossell, R. Erni, R. Caputo, L. Protesescu, K. V. Kravchik, D. N. Dirin, K. Lienau, F. von Rohr, *et al.*, *J. Am. Chem. Soc.* **136**, 12422 (2014).
- F. Gonella, G. Mattei, P. Mazzoldi, E. Cattaruzza, G. W. Arnold, G. Battaglin, P. Calvelli, R. Polloni, R. Bertonecello and R. F. Haglund Jr., *Appl. Phys. Lett.* **69**, 3101 (1996).
- H. Kurita, A. Takami and S. Koda, *Appl. Phys. Lett.* **72**, 789 (1998).
- J. Bosbach, D. Martin, F. Stietz, T. Wenzel and F. Trager, *Appl. Phys. Lett.* **74**, 2605 (1999).
- K. F. MacDonald, V. A. Fedotov, S. Pochon, K. J. Ross, G. C. Stevens, N. I. Zheludev, W. S. Brocklesby and V. I. Emel'yanov, *Appl. Phys. Lett.* **80**, 1643 (2002).
- V. A. Fedotov, K. F. MacDonald, N. I. Zheludev and V. I. Emel'yanov, *J. Appl. Phys.* **93**, 3540 (2003).
- A. V. Krasavin, K. F. MacDonald, N. I. Zheludev and A. V. Zayats, *Appl. Phys. Lett.* **85**, 3369 (2004).
- P. J. Bennett, S. Dhanjal, P. Petropoulos, D. J. Richardson, N. I. Zheludev and V. I. Emel'yanov, *Appl. Phys. Lett.* **73**, 1787 (1998).
- K. F. MacDonald, V. A. Fedotov and N. I. Zheludev, *Appl. Phys. Lett.* **82**, 1087 (2003).
- R. Kofman, P. Cheyssac and J. Richard, *Phys. Rev. B* **16**, 5216 (1977).
- N. R. Comins, *Phil. Mag.* **25**, 817 (1972).

29. A. García-Marín, M. J. Hernández, E. Ruiz, J. M. Abad, E. Lorenzo, J. Piqueras and J. L. Pau, *Biosensors and Bioelectronics* **74**, 1069 (2015).
30. M. W. Knight, T. Coenen, Y. Yang, B. J. M. Brenny, M. Losurdo, A. S. Brown, H. O. Everitt and A. Polman, *ACS Nano* **9**, 2049 (2015).
31. A. Defrain, *J. Chim. Phys.* **74**, 851 (1977).
32. G. Fritsch and E. Luscher, *Phil. Mag. A* **48**, 21 (1983).
33. A. Di Cicco, S. Fusari and S. Stizza, *Phil. Mag. B* **79**, 2113 (1999).
34. A. Di Cicco, R. Gunnella, R. Marassi, M. Minicucci, R. Natali, G. Pratesi, E. Principi and S. Stizza, *J. Non-Cryst. Solids* **352**, 4155 (2006).
35. X. F. Li, G. T. Fei, X. M. Chen, Y. Zhang, K. Zheng, X. L. Liu and L. D. Zhang, *Europhys. Lett.* **94**, 16001 (2011).
36. M. Losurdo, A. Suvorova, S. Rubanov, K. Hingerl and A. S. Brown, *Nat. Mater.* **15**, 995 (2016).
37. L. Holland, in *Vacuum deposition of thin films* (Chapman and Hall Ltd., London, 1963), pp. 199.
38. E. Søndergård, R. Kofman, P. Cheyssac and A. Stella, *Surf. Sci.* **364**, 467 (1996).
39. B. El Roustom, G. Fôti and C. Cominellis, *Electrochem. Commun.* **7**, 398 (2005).
40. P. Meakin, *Rep. Prog. Phys.* **55**, 157 (1992).
41. J. Schindelin, I. Arganda-Carreras, E. Frise, V. Kaynig, M. Longair, T. Pietzsch, S. Preibisch, C. Rueden, S. Saalfeld, B. Schmid, *et al.*, *Nat. Meth.* **9**, 676 (2012).
42. P. G. de Gennes, *Rev. Mod. Phys.* **57**, 827 (1985).
43. M. J. Regan, H. Tostmann, P. S. Pershan, O. M. Magnussen, E. DiMasi, B. M. Ocko and M. Deutsch, *Phys. Rev. B* **55**, 10786 (1997).

ACCEPTED MANUSCRIPT

